Journal of Molecular Liquids 286 (2019) 110915

Contents lists available at ScienceDirect

Journal of Molecular Liquids

journal homepage: www.elsevier.com/locate/molliq

Experimental and computational chemistry studies of two imidazole-based compounds as corrosion inhibitors for mild steel in HCl solution

Mahla Talari [a], Siavosh Mozafari Nezhad [a], Seyed Jamal Alavi [b], Mostafa Mohtashamipour [a], Ali Davoodi [a,*], Saman Hosseinpour [c,*]

[a] Materials and Metallurgical Engineering Department, Faculty of Engineering, Ferdowsi University of Mashhad, Mashhad, Iran
[b] Department of Chemistry, Faculty of Science, Ferdowsi University of Mashhad, Mashhad, Iran
[c] Institute of Particle Technology (LFG), Friedrich-Alexander-Universität-Erlangen-Nürnberg (FAU), Cauerstraße 4, 91058 Erlangen, Germany

ARTICLE INFO

Article history:
Received 15 February 2019
Received in revised form 12 April 2019
Accepted 2 May 2019
Available online 3 May 2019

Keywords:
Inhibitors
Thiazole-based compounds
Electrochemical impedance spectroscopy
Monte Carlo simulation
Density functional theory

ABSTRACT

Two imidazole-based corrosion inhibitors, namely thiazole-4-carboxylic acid (TCA) and 2-methyl-1,3-thiazole-4-carboxylic acid (MTCA), were synthesized and their corrosion inhibition performance on mild steel in 0.1 mol·L^{-1} HCl solution at 25 °C was investigated using electrochemical measurements. Corrosion inhibition efficiency increased with increasing inhibitor concentration in solution and at a concentration of 150 ppm, both MTCA and TCA exhibited similar corrosion inhibition efficiencies of ~90%. Adsorption of both inhibitors on steel followed the Langmuir adsorption isotherm. Theoretical quantum chemical calculation and Monte Carlo simulation were employed to determine the most stable configuration, the adsorption sites, and the interaction energies of TCA and MTCA on the steel surface. The simulation results demonstrated that the competitive adsorption of inhibitors and water molecules, proton, and chloride ions has a large impact on the adsorption configuration of inhibitors.

1. Introduction

Metal deterioration through corrosion leads to an immense economic loss, which is a major concern in the industrial application of metals, especially in acidic media. Therefore, there is a high demand for developing methods for preventing corrosion or reducing its rate. Applying small quantities of organic compounds as inhibitors to a solution is a practical method through which corrosion can be prevented by controlling the dissolution of metals. The inhibition efficiency of an inhibitor in a given environment is greatly affected by its chemical structure and its interaction with the metal surface. Many heterocyclic compounds containing nitrogen, sulfur, oxygen, and π-bonds are known to be effective inhibitors of steel corrosion, since they adsorb on the metal surface and form an effective barrier film [1–6]. Studies have revealed that the formation of donor-acceptor complexes between inhibitors and the metal surface is the main mechanism through which inhibitors typically protect metal surfaces. Thus, inhibition efficiency closely depends upon structural parameters including the functional groups of the inhibitor, the electron density at the donor atoms as well as the electronic structure of the adsorbed molecules/substrate [7–10]. In this regard, imidazole-based corrosion inhibitors are among the most effective corrosion inhibitors for copper, zinc, and steel and their protection efficacy has been investigated both experimentally and theoretically.

In recent years, theoretical approaches have received increased attention in fundamental corrosion studies [11,12]. Monte Carlo (MC) simulation and quantum chemical calculation, for instance, have been used to study the molecular structures of inhibitors and their interactions with metal substrates at a molecular level, which is essential for understanding the inhibition performance of adsorbates [13–21]. Different inhibition efficiencies of various organic inhibitors are demonstrated by illustrating the optimum configuration of the organic molecules adsorbed onto the metal surface and by computing their interaction energies [22–25]. For instance, Gou et al. [26] investigated the inhibition efficiency of triazole derivatives on the corrosion of mild steel using quantum chemical and MC simulation and found out that the triazole derivatives are adsorbed on mild steel surface directly via sharing electrons with iron atoms.

A major concern regarding the theoretical calculation of corrosion inhibitors is that they are mostly implemented in a vacuum condition without considering competition and/or co-adsorption among inhibitor molecules and aqueous constituents (e.g. water, acid molecules, and ions) [27–29]. Such competitive adsorption may completely change the configuration of adsorbed molecules on a surface. For instance, we showed in our previous work [22] that Clopidogrel, a cardiovascular drug class that can be used as a green corrosion inhibitor, adopts a flat

* Corresponding authors.
E-mail addresses: a.davodi@um.ac.ir (A. Davoodi), saman.hosseinpour@fau.de (S. Hosseinpour).

https://doi.org/10.1016/j.molliq.2019.110915
0167-7322/

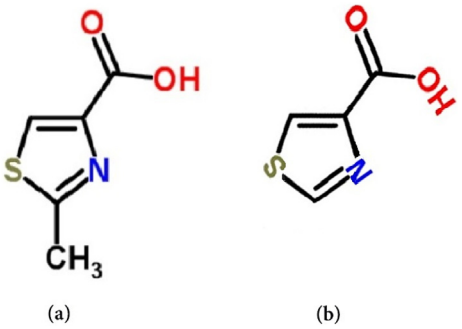

Fig. 1. Chemical structure of a) 2-methyl-1,3- thiazole-4-carboxylic acid (MTCA) and b) thiazole-4-carboxylic acid (TCA).

configuration in the absence of water molecules while in an aqueous medium Clopidogrel replaces water molecules and adsorbs with one of its rings perpendicular to the sample surface, consistent with experimental results. Moreover, there has been little investigation on the influence of interactions between inhibitors with the surface under investigation [6,29,30].

In the present study, we investigate the corrosion inhibition efficiencies of two imidazole-based organic compounds, namely thiazole-4-carboxylic acid (TCA) and 2-methyl-1,3-thiazole-4-carboxylic acid (MTCA), on carbon mild steel in 0.1 mol·L^{-1} HCl solution using potentiodynamic polarization and electrochemical impedance spectroscopy (EIS). We further performed quantum chemical calculation and MC simulation, to elucidate the adsorption behavior of the inhibitors on the metal surface in the presence and absence of solution constituents.

2. Experimental

2.1. Electrochemical evaluations

A commercially available mild steel (composition: Mn (0.6 wt%), P (0.36 wt%), C (0.15 wt%), Si (0.03 wt%), and Fe (balance)) with a surface area of 1 cm^2 was used as the working electrode for the electrochemical evaluations. The surface of the working electrode was mechanically abraded with emery paper up to 1200 grit, cleaned with distilled

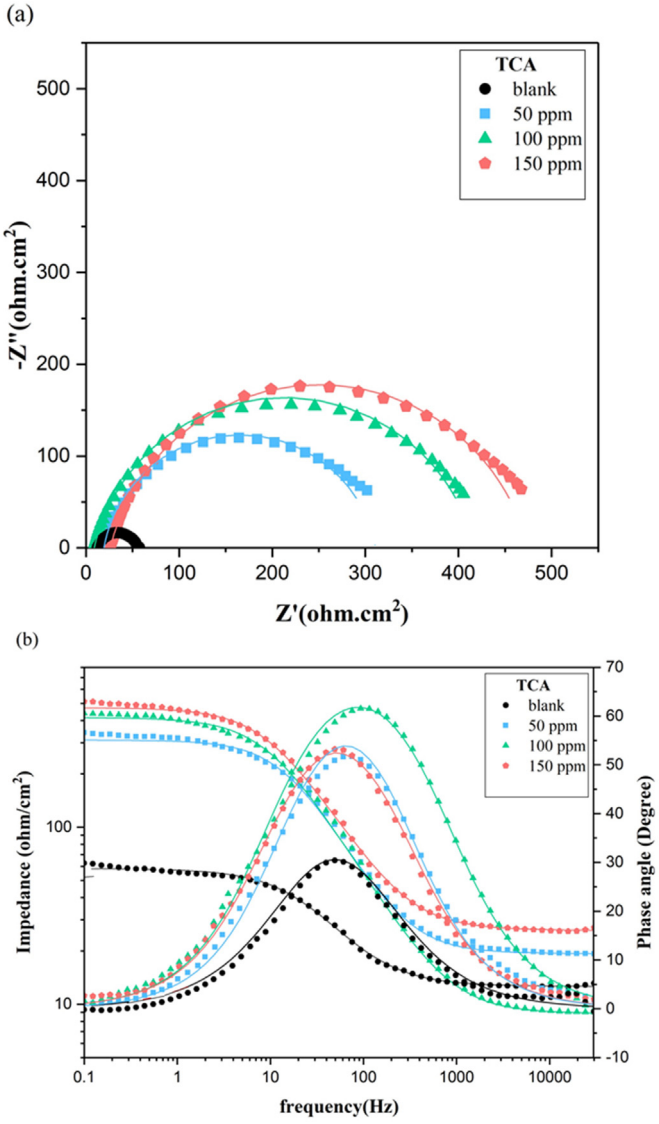

Fig. 2. a) Nyquist and b) Bode plots of mild steel in 1.0 mol·L^{-1} HCl solution containing different concentrations TCA inhibitor. Lines are the fits to the experimental data (symbols).

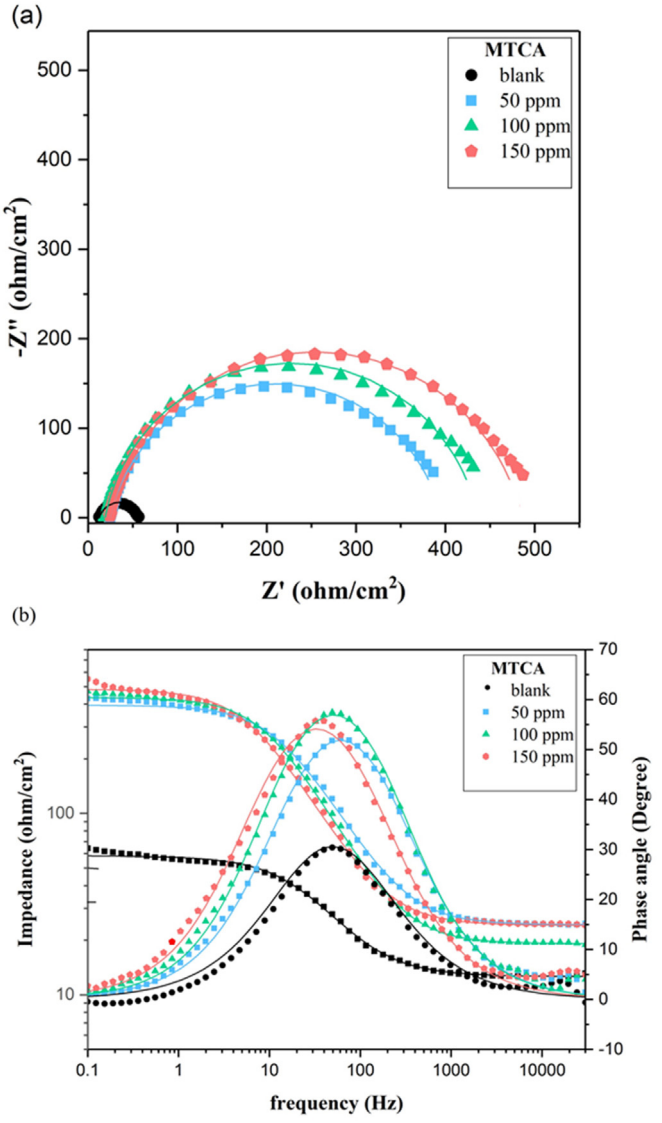

Fig. 3. a) Nyquist and b) Bode plots of mild steel in 1.0 mol·L^{-1} HCl solution containing different concentrations MTCA inhibitor. Lines are the fits to the experimental data (symbols).

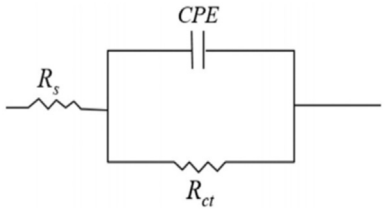

Fig. 4. Electrical equivalent circuit used to fit the impedance data.

water, and dried in room temperature prior to the electrochemical measurements.

HCl (Merck 37%) was diluted with distilled water to prepare a 0.1 mol·L^{-1} HCl solution. TCA and MTCA, were synthesized according to the procedure presented in the supplementary material and were added as inhibitors to the corrosive solution in concentrations of 50, 100 and 150 ppm. Fig. 1 illustrates the chemical structure of these inhibitors. The acid solution in the absence of the inhibitors was considered as blank for comparison.

The three electrodes cell assembly with the mild steel as the working electrode, a saturated Calomel electrode as the reference electrode, and a platinum mesh electrode as an auxiliary electrode was used for the EIS and potentiodynamic polarization studies. The Electrochemical measurements were carried out using a Gill AC laboratory potentiostat (ACM instrument). The experiments were performed after the stabilization of the system (i.e. 1 h after immersion). Potentiodynamic polarization measurements were performed at a constant sweep rate of 1 mV·s^{-1} in the scanning range from −250 to +250 mV, with respect to the open circuit potential (OCP). EIS measurements were performed in the frequency range from 0.1 to 30,000 Hz, using an AC perturbation amplitude of ±10 mV. EIS spectra were analyzed using the Spectrum Analyzer software.

2.2. DFT calculation and MC simulation

Quantum chemical calculation was performed using the Gaussian 09 software [31]. The input file for the construction of the inhibitor molecules, was prepared using Gauss View 5.0.8 [31]. A full optimization was implemented in a DFT (density functional theory) method, combined with B3LYP/6-311G ++ (d,p) basis set. The B3LYP is known to provide accurate electronic properties and geometries for a wide range of organic compounds and has been previously used in studying the adsorption of corrosion inhibitors from solutions [26,32–34]. The energy of the highest occupied molecular orbital (E_{HOMO}), the energy of the lowest unoccupied molecular orbital (E_{LUMO}), the energy gap (i.e. $\Delta E = E_{LUMO}$-E_{HOMO}), the dipole moment (μ), and Mulliken charge were determined in the quantum chemical simulation.

MC simulation was conducted using material studio 8.0 software (Accelrys Inc.) [35] to calculate the interaction energies between TCA or MTCA molecules with the Fe surface, using the absorption locator module. This module also identifies the possible adsorption sites and the inhibitors' best adsorption configurations on the surface, as the temperature is slowly lowered in the simulation box.

To start with the simulation, a Fe substrate with either open structure (−100) plane or closely packed (110) plane was constructed from the cleavage of a Fe crystal and the surface structure was optimized to minimize the total energy. The simulation process was carried out in a simulation box (24.3A° × 24.3A° × 45.7A°) with a periodic boundary condition, to model the representative part of the interface. Therefore, the arbitrary boundary effect can be neglected. Six layers of Fe atoms were selected in the simulation box. The Fe layers were chosen deep enough so that the inhibitor molecules will be only involved in the non-bond interactions with the Fe surface atoms. The absorption configurations of the TCA and MTCA molecules on the Fe substrate were simulated using COMPASS (Condensed-phase Optimized Molecular Potentials for Atomistic Simulation Studies) force field in the simulation box containing the inhibitor molecules, the electrolyte, and water molecules. The surface potential energy, on which the atomic nuclei move, was represented by classical force fields. The classical force fields were assembled by a parameter set which was derived from experiments and high-level quantum mechanical calculation to approximate these studies [26,36]. In the course of the simulation, the adsorbed molecules were randomly rotated and transferred around the substrate as the temperature was slowly lowered, in order to identify the global low-energy adsorption sites.

3. Results and discussion

3.1. Electrochemical measurements

3.1.1. EIS measurements

The EIS results obtained on mild steel in solutions containing different concentrations of TCA inhibitor and a solution without any inhibitor (denoted as blank for comparison) are plotted in Fig. 2a and b with Nyquist and Bode representations, respectively. Similar measurements were performed on samples in solutions containing various concentrations of MTCA and the corresponding results are presented in Fig. 3a and b. The bode plots of MTCA and TCA inhibitors (Figs. 2b and 3b) show that the addition of the inhibitors increases the impedance, especially in low frequency domains. The values of phase angles at higher frequency domains are attributed to the capacitive behavior of the inhibitors. The negative values of phase angle reflect the dominant capacitive behavior of the inhibitors after adsorption to the surface. The EIS experimental data were fitted using an equivalent circuit model as depicted in Fig. 4. The use of a constant phase element (CPE) instead of the capacitance was essential to better fit the experimental results, which reflects the surface heterogeneity [37]. The CPE is defined in Eq. (1): [38].

$$Z(\omega) = Y_\circ (j\omega)^{-n} \tag{1}$$

Table 1
Electrochemical impedance parameters obtained in the present and absence of inhibitors in 0.1 mol.L^{-1} HCl solution.

Inhibitor	Concentration (ppm)	R_s ($\Omega \cdot cm^2$)	R_{ct} ($\Omega \cdot cm^2$)*	CPE_{dl}		C_{dl} (μF cm^{-2})	IE%
				P (μS cm^{-2})	n × 100		
Blank	–	12.66 ± 0.73	43.40 ± 0.13	376.3 ± 10.16	83.6 ± 0.41	162.00	–
TCA	50	19.29 ± 0.34	291.66 ± 9.04	64.4 ± 1.7	89.3 ± 0.40	39.40	85.1
	100	8.82 ± 0.21	408.30 ± 10.98	73.4 ± 1.79	86.7 ± 0.35	41.46	89.3
	150	26.05 ± 0.55	448.3 ± 15.24	67.8 ± 1.96	85.4 ± 0.46	36.60	90.3
MTCA	50	24.27 ± 0.40	371.40 ± 8.54	63.9 ± 1.46	86.4 ± 0.36	34.75	88.3
	100	19.21 ± 0.34	418.69 ± 10.04	72.2 ± 1.66	89.90.38	46.85	89.6
	150	23.92 ± 0.69	491.99 ± 9.80	138.0 ± 5.10	84.43 ± 0.59	64.62	91.1

* R_{ct} is corrected for the solution resistance and the corresponding IE% are calculated accordingly.

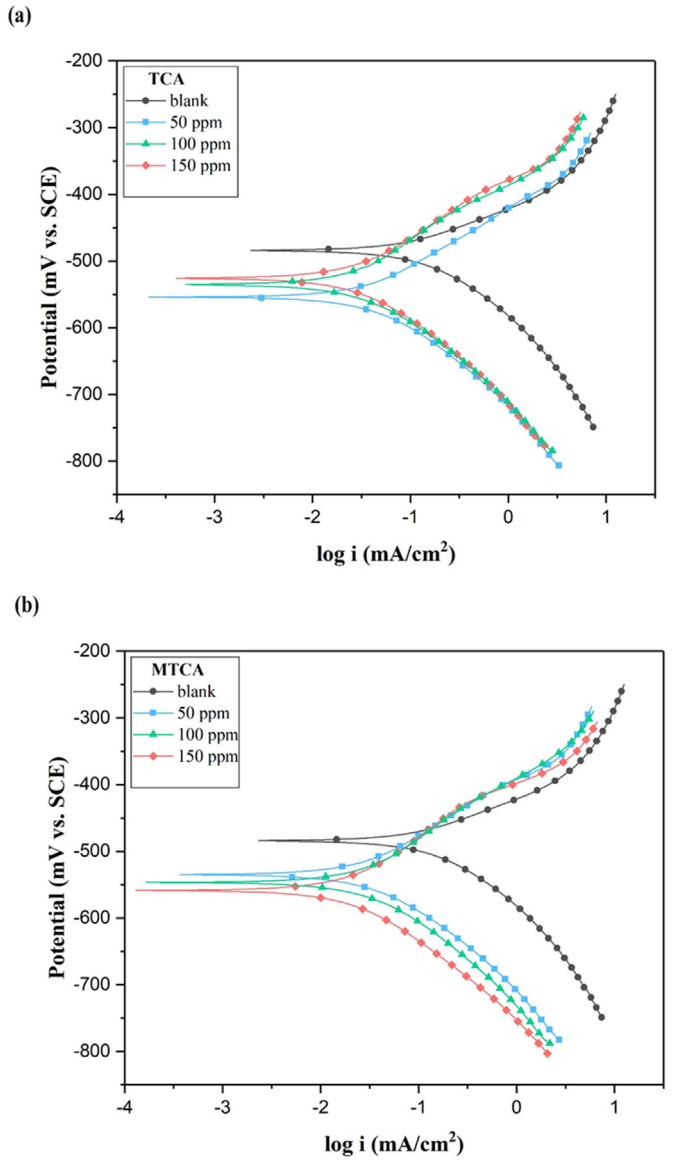

Fig. 5. Potentiodynamic polarization curves for mild steel in 0.1 mol·L^{-1} HCl with various concentration of (a) TCA and (b) MTCA inhibitors.

where Y_0 and ω are the CPE constant and the angular frequency (in rad.s^{-1}), respectively. $j^2 = -1$ is an imaginary number and *n* is the CPE exponent. The capacitance (C) associated with constant phase element (CPE_{dl}) is hence calculated using Eq. (2) where R_{ct} denotes the charge transfer resistance: [39].

$$C = \left(Y_\circ R_{ct}^{1-n}\right)^{-1/n} \tag{2}$$

The inhibition efficiencies (IE%) of the inhibitors were calculated from the impedance parameters, as described in Eq. (3): [40].

$$IE(\%) = \left(\frac{(R_{t,i} - R_{t,0})}{R_{t,i}}\right) \times 100 \tag{3}$$

where $R_{t,i}$ and $R_{t,0}$ are the charge transfer resistances with and without the inhibitors, respectively.

All impedance parameters including R_{ct}, solution resistance (R_s), double layer capacitance (C_{dl}), and IE% are summarized in Table 1. This table indicates that the addition of inhibitors to the solution results in a considerable increase in the value of R_{ct}. Adsorption of the inhibitors on the metal surface leads to either an increase in the electronic double layer thickness or a decrease in the local dielectric constant, both of which lead to a decrease in the C_{dl} value [30,41,42]. Increasing the charge transfer resistance can be correlated to the formation of a protective film at the metal/solution interface. The R_{ct} and consequently IE% increase upon increasing the concentration of inhibitors. In all concentrations MTCA provides only a slightly higher protection efficiency, compared to TCA despite their different chemical structure. Both inhibitor molecules prohibit corrosion reactions by direct chemical adsorption on the metal surface via sharing electrons with the substrate, as will be discussed later.

3.1.2. Potentiodynamic polarization measurements

Fig. 5a and b depict the potentiodynamic polarization curves for mild steel in 0.1 mol.L^{-1} HCl solution in the absence and presence of TCA and MTCA inhibitors, respectively. Tafel line extrapolation was used to obtain the quantitative electrochemical parameters, including corrosion potential (E_{corr}), corrosion current density (i_{corr}), cathodic and anodic Tafel slopes (β_c and β_a). The results from potentiodynamic measurements are summarized in Table 2. The IE% and surface coverage (θ) of the inhibitors are also calculated according to Eq. (4) and Eq. (5) [29] and the obtained values are presented in Table 2.

$$\Theta = \frac{(i_{corr} - i_{corr(inh)})}{i_{corr}} \tag{4}$$

$$IE(\%) = \frac{(i_{corr} - i_{corr(inh)})}{i_{corr}} \times 100 \tag{5}$$

where i_{corr} and $i_{corr(inh)}$ are current density values without and with inhibitors, respectively.

Adsorption of the inhibitors on a metal surface often leads to a reduction of the number of active reaction sites, as they are blocked by adsorbates. The lower number of active sites on the metal surface yields a lower metal dissolution and/or hydrogen evolution during the electrochemical reaction. As shown in Table 2, adding inhibitors to the solution changes both anodic and cathodic slopes compare to those of the blank solution, which points to the fact that both TCA and MTCA act as mixed-type inhibitors [30,37,43,44]. Additionally, the corrosion current density decreases (the inhibition efficiency increases) as the inhibitor

Table 2
Electrochemical parameters obtained from the potentiodynamic polarization curves (results from Fig. 5).

Inhibitor	Concentration (ppm)	β_a (mV/decade)	$-\beta_c$ (mV/decade)	i_{corr} (mA cm^{-2})	E_{corr} (mV vs. SCE)	Θ	IE%
Blank	–	65.62	145.92	0.21	−473.51	–	–
TCA	50	84.91	127.71	0.04	−553.67	0.80	80
	100	87.61	120.56	0.03	−534.04	0.87	87
	150	86.55	120.26	0.02	−526.26	0.90	90
MTCA	50	83.41	126.15	0.03	−534.74	0.86	86
	100	86.56	111.58	0.02	−547.03	0.90	90
	150	97.82	113.60	0.01	−558.73	0.92	92

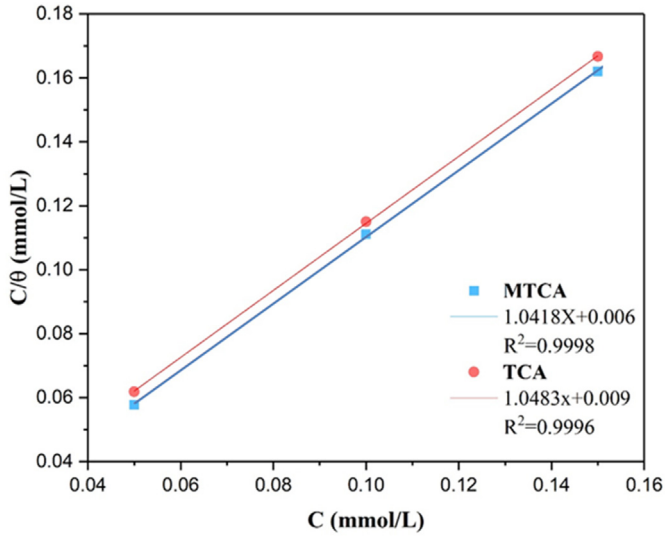

Fig. 6. Adsorption isotherm on mild steel in 1.0 mol.L^{-1} HCl solution containing different concentrations of MTCA and TCA. The lines are fit to the Langmuir isotherm model (Eq. 6).

concentration increases for both inhibitors. The corrosion current density, which is the main criterion in determining the inhibiting properties of an inhibitor, in the solution containing MTCA is only slightly lower than that of the solution containing TCA, under the similar concentration in an agreement with our EIS results, vide infra. As it is clear from Tables 1 and 2, the inhibition efficiency values obtained from both potentiodynamic polarization and EIS measurements are comparable. The hydrophobic methyl group in MTCA (illustrated in Fig. 1) could potentially contribute to the better corrosion protection efficiency of MTCA compared to TCA. However, as it was evident with the MC simulation (Section 3.3), both inhibitors adsorb with their carboxyl groups away from the substrate, minimizing the effect of hydrophobic tail of MTCA.

Table 3
Quantum chemical parameters calculated using the B3LYP method with a 6–311G++ (d, p) basis set for MTCA and TCA molecules.

Inhibitor	E_{HOMO} (eV)	E_{LUMO} (eV)	ΔE (eV)	μ(Debye)	ΔN
TCA	−0.2688	−0.07584	0.2091	4.8339	23.375
MTCA	−0.2303	−0.09152	0.1387	2.3794	49.280

3.1.3. Adsorption isotherm

During the adsorption of an inhibitor on a surface, multiple interactions are expected between the inhibitor molecules, between the inhibitor and competing co-adsorbing molecules (e.g. water), and between inhibitor and surface. Studying adsorption isotherm is a useful method to investigate these interactions and revealing the inhibitors' adsorption mechanism [36]. We, thus, studied the adsorption isotherm of MCTA and TCA on steel surface by following their surface coverage (Θ) as a function of inhibitor's concentration in the 0.1 mol·L^{-1} HCl solution (C_{inh}). The plots in Fig. 6 demonstrate that both TCA and MTCA inhibitors follow the linear Langmuir isotherm trend, as the plots yield straight lines with the correlation coefficient of approximately 1. The Langmuir isotherm is defined as the following: [26].

$$\frac{C_{inh}}{\theta} = \frac{1}{K_{ads}} + C_{inh} \tag{6}$$

Here, K_{ads} denotes the equilibrium constant for adsorption and Θ is calculated from potentiodynamic polarization measurements. The free adsorption energy (ΔG°_{ads}) relates to K_{ads} through Eq. (7): [36,45].

$$\Delta G^{\circ}_{ads} = -RTln(55.5\ K_{ads}) \tag{7}$$

where R is the gas constant, T is the temperature and 55.5 is the molar concentration of water in solution (expressed in mol·L^{-1}). In the Langmuir adsorption model inhibitors are assumed to adsorb on a solid surface with series of distinct binding sites, where all the sites are equivalent and each site can bind to only one inhibitor.

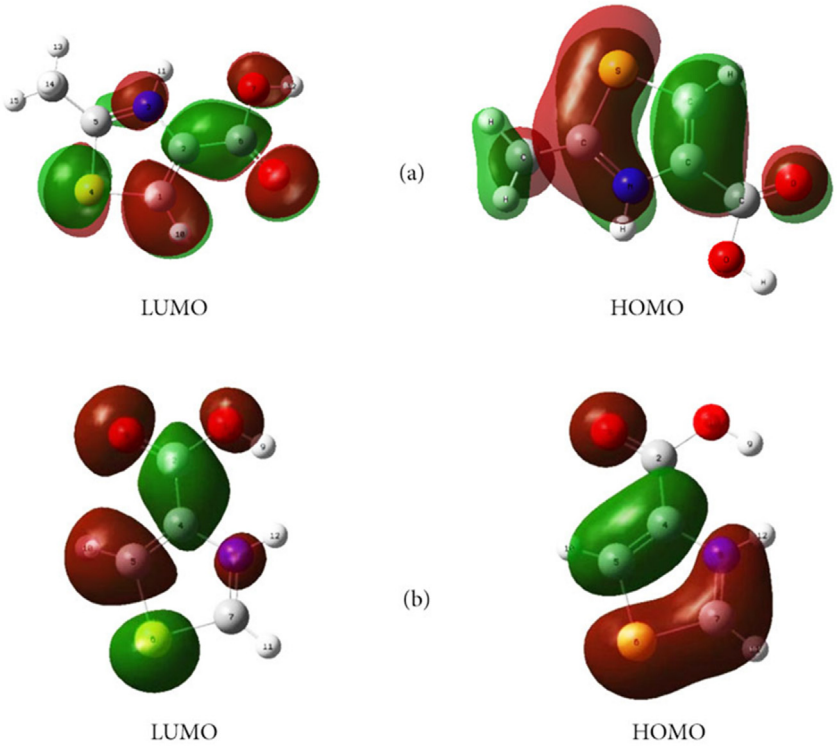

Fig. 7. Highest occupied molecular orbital (HOMO) and lowest unoccupied molecular orbital (LUMO) for (a) MTCA and (b) TCA molecule, calculated using DFT/B3LYP/6–31++G(d,p).

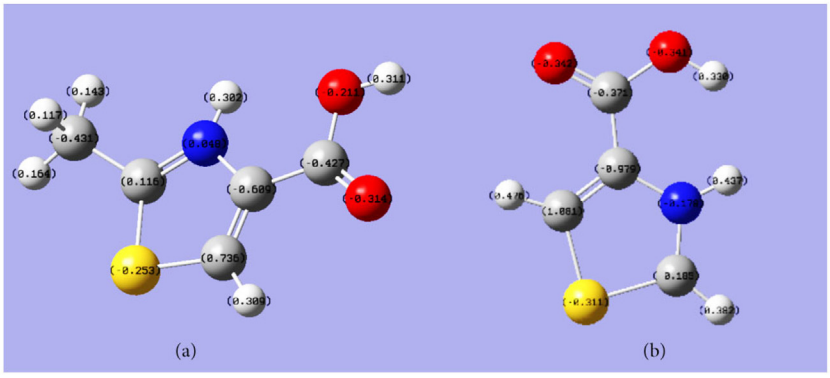

Fig. 8. Distribution of Mulliken charges in (a) MTCA and (b) TCA inhibitors.

In general, ΔG°_{ads} less than $-40\ kJ\cdot mol^{-1}$ is an indication of a pure chemisorption of adsorbates on a surface [45], while larger ΔG°_{ads} values point toward contribution of physisorption in the adsorption process. The calculated ΔG°_{ads} for MTCA and TCA are $-34.36\ kJ\cdot mol^{-1}$ and $-34.34\ kJ\cdot mol^{-1}$, respectively. It is thus evident that both inhibitors adsorb by a chemi-physisorption on the metal surface possibly through their lone pair electrons. To provide a deeper insight into the adsorption mechanism of the two imidazole-based inhibitors, we performed quantum chemical calculation.

3.2. Quantum chemical calculation

The spatial molecular structure of an inhibitor as well as its electronic structure play key roles in the inhibition efficiency of the molecule. Frontier orbital theory is proven to be helpful in unraveling the interaction mechanisms of the inhibitor molecules with metal surfaces [46,47]. In Fig. 7 we have shown the HOMO and LUMO of MTCA and TCA in their optimized form, using the B3LYP method with a 6–311G++ (d, p) basis set. The calculated quantum parameters for both inhibitors are listed in Table 3. The impact of E_{HOMO} and E_{LUMO} of inhibitors, which govern the ability of the inhibitor molecules to react with a substrate, are discussed as follows. E_{HOMO} indicates the electron donating ability of a molecule. The high values of E_{HOMO}, in the present case, mean that the inhibitors can offer electrons to the unoccupied *d* orbital of the substrate (i.e. iron atoms in this case) more easily. This facilitates the adsorption of the inhibitor on the surface and therefore increases the adsorbates' inhibition efficiency [29]. The E_{LUMO}, on the other hand, indicates the electron accepting ability of the inhibitor. Accumulation of electrons on the surface results in the repellence of the electronegative inhibitor from the surface and therefore decreases its corrosion inhibition efficiency. In the present study, the low value of E_{LUMO} indicates that inhibitor can easily accept free electrons from metal. Therefore, the charge of the metal surface remains redundant with an enhanced inhibition efficiency [29], which agrees with the high IE % that are obtained experimentally.

The energy gap ($\Delta E = E_{HOMO}$-E_{LUMO}) is another important quantity that is often used in assessing the binding ability of the inhibitor molecules on metal surfaces [46,48]. An inhibitor with a small energy gap is associated with a high inhibition efficiency, as less energy is required to remove electrons from the last occupied orbital and the inhibitor adsorbs on the metal surface more readily [6,37,45,49]. According to Table 3, MTCA shows a lower ΔE compared to TCA. MTCA also has higher E_{HOMO} and lower E_{LUMO} values compared to TCA. Nevertheless, the two inhibitors show comparable inhibition efficiencies, with MTCA being only slightly more efficient than TCA. The HOMO of inhibitors appears mainly in the vicinity of sulfur, nitrogen and oxygen atoms, facilitating their adsorption on the surface via these atomic sites. A similar conclusion is obtained considering the charge distribution over both inhibitor molecules, using the Mulliken charge population analysis [29,50] (results in Fig. 8). As shown in this figure, the highest negative charge densities are placed on sulfur, nitrogen and oxygen atoms, which result in a strong bond between the inhibitor and the metal surface through these atoms. In addition, the adsorption occurs through these atoms with the highest negative charge density, consistent with previous studies [29,48,50].

The fraction of electrons transferred from the inhibitor molecules to the metal atoms (ΔN) may be calculated using Eq. (8): [29,30,37].

$$\Delta N = \frac{(X_{Fe-X_{inh)}})}{2(\eta_{Fe}-\eta_{inh})} \tag{8}$$

where X_{Fe} and X_{inh} represent the absolute electronegativity of iron and the inhibitor molecule, respectively. η_{Fe} and η_{inh} denote the absolute hardness of iron and the inhibitor molecule, respectively. The theoretical values of X_{Fe} and η_{Fe} are 7 and 0 $eV\cdot mol^{-1}$, respectively [30]. These quantities for the inhibitor molecules may be calculated from the quantum chemical calculation as follows:

$$X_{inh} = \frac{-(E_{HOMO}-E_{LUMO})}{2} \tag{9}$$

$$\eta_{inh} = \frac{-(E_{HOMO}+E_{LUMO})}{2} \tag{10}$$

Table 4
Outputs and descriptors calculated by the MC simulation for adsorption of MTCA and TCA molecules on Fe (−100) and Fe (110), in the presence and absence of water and acid.

System	Total energy ($kcal\cdot mol^{-1}$)	Adsorption energy ($kcal\cdot mol^{-1}$)	Rigid adsorption energy ($kcal\cdot mol^{-1}$)	Deformation energy ($kcal\cdot mol^{-1}$)	dE_{ad}/dN_i inhibitor ($kcal\cdot mol^{-1}$)	Rotate degrees
Fe (−100)/MTCA	28.752	−26.162	−2.229	−23.933	−26.162	6.712
Fe (−100)/TCA	18.170	−16.377	−2.646	−13.690	−16.337	5.377
Fe(−100)/MTCA/Water/Acid	−40.361	−920.218	−71.394	−848.824	−35.94	13.674
Fe (−100)/TCA/Water/Acid	−48.7123	−908.163	−69.62	−838.500	−28.105	12.16
Fe (110)/MTCA	17.648	−16.860	−3.171	−13.688	−16.860	2.927
Fe (110)/TCA	9.054	−2.620	−2.621	-4.504×10^{-4}	−2.620	6.245
Fe(110)/MTCA/Water/Acid	−169.806	-1.831×10^{3}	−181.558	-1.649×10^{3}	−19.198	11.82
Fe (110)/TCA/Water/Acid	−167.143	-1.828×10^{3}	−179.068	-1.649×10^{3}	−12.511	12.87

The dominant factor affecting the inhibition efficiency is the transfer of electrons from the inhibitor molecules to the metal surface, which occurs through electron donation [29,34,45]. The electron transfer through the adsorbed layer can also be promoted by increasing the dipole moment values, although this correlation has not been completely understood [45]. To further unravel the adsorption configuration of inhibitors, we performed MC simulation.

3.3. MC simulation

MC simulation was employed to determine the most stable adsorption configuration of the inhibitors on the iron surface, in the presence and absence of water and acid in the simulation box. The adsorption energy distribution of the optimized TCA/iron system and MTCA/iron system including total energy, average total energy, van der Waals energy,

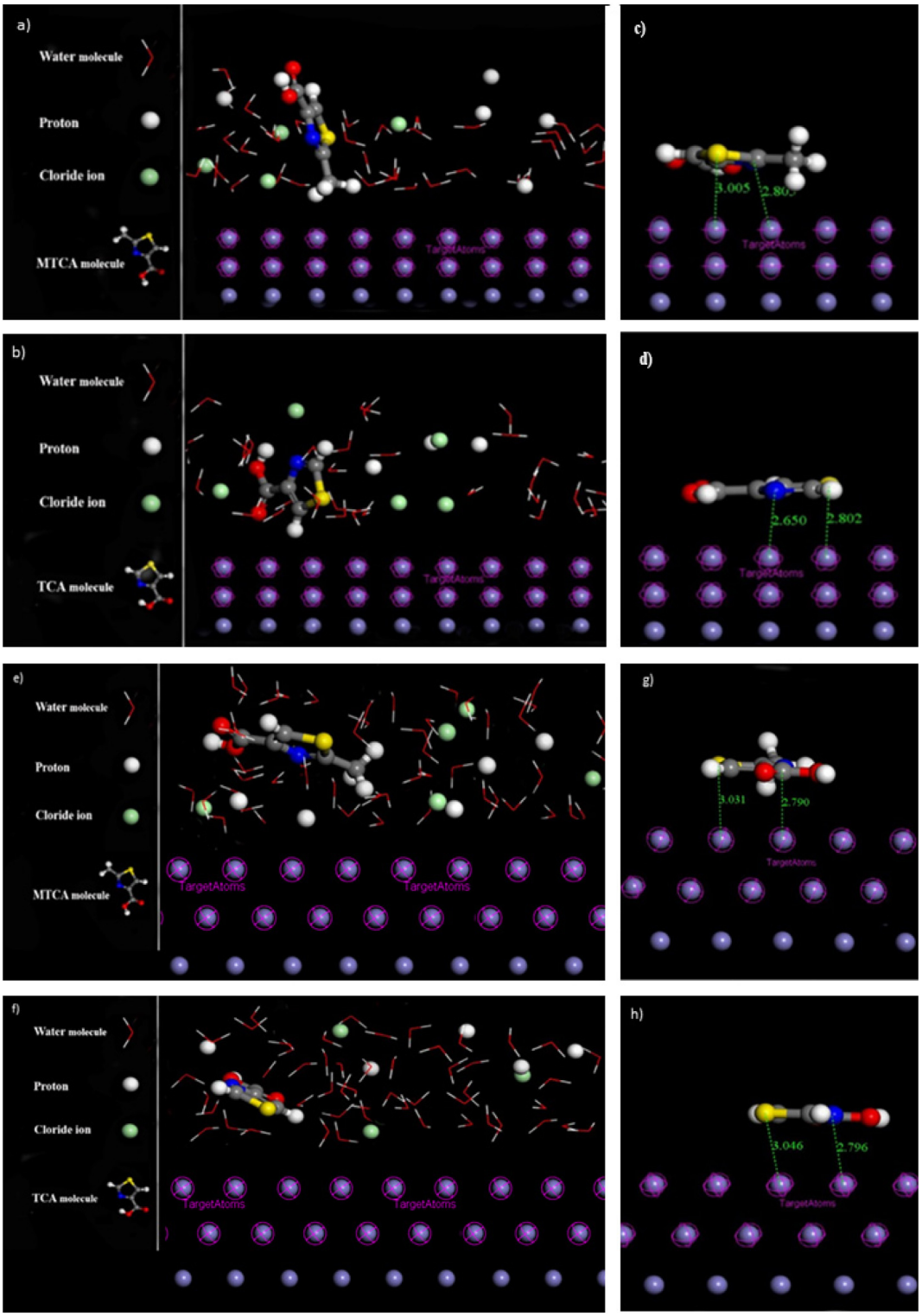

Fig. 9. Adsorption configuration of (a) MTCA and (b) TCA inhibitors on Fe (−100) in the presence of water molecules, the protons, and the chloride ions. (c) and (d) depict the adsorption configuration of MTCA and TCA inhibitors on Fe (−100) in the absence of water or acid, respectively. Corresponding results for the adsorption of inhibitors on Fe (110) are presented in panels e–h.

electrostatic energy, and intermolecular energy of interacting species were also determined in MC simulation. The closely packed Fe (110) plane has been showed to be the most preferable plane to represent iron surface. [26] Nevertheless, for comparison and to account for the less packed crystalline planes, we performed similar simulation on (−100) plane as well. Table 4 displays the output values calculated from MC simulation of inhibitor adsorption on the iron surface in the systems containing water and acid and the systems containing only the inhibitors. The iron surface energy is assumed zero in all the calculation. The adsorption parameters (all in Kcal·mol^{-1} units) were determined as follows: The total energy is defined as the sum of the adsorption energy and the internal energy of adsorbed components. The adsorption energy is composed of the adsorption energy of the adsorbed components in input configuration and the diminutive deformation energy, which is the energy associated with the relaxation of the adsorbed components in the presence of the surface. The rigid adsorption energy is the energy released (or required) when the adsorbed components are adsorbed onto the metal surface, before geometrical optimization [19,35,51]. Table 4 also shows the differential energy (dE_{ads}/dN_i) which indicates the energy on which a particular adsorbed component requires to be removed from surface. The most stable configuration of inhibitor molecules is the one with the least total adsorption energy. According to Table 4, in the presence of water and acid, the total adsorption energies are comparable for both inhibitors, reflecting their comparable inhibition efficiency in agreement with the electrochemical results.

Adsorption of an organic inhibitor, as a protective layer, on a metal surface inhibits the metal from corrosion corrosive solutions. As was mentioned earlier, the conformation of inhibitor affects the protection efficiency of the inhibitor. The conformation of inhibitor when adsorbed on a surface depends upon the inhibitor's structure, metal surface properties (e.g. packing density), as well as the competitive adsorption of inhibitor and other constituents of the solution. Fig. 9a and b respectively depict the most stable configuration of MTCA inhibitor at the vicinity of Fe (−100) surface in the simulation box containing water and acid (H^+ and Cl^-) and the system of MTCA/iron alone. Corresponding results for the system containing TCA are presented in Fig. 9c and d. Similarly, the simulation results for adsorption of inhibitors on the closely packed Fe (110) surface are also provided in Fig. 9e–h, for comparison. It is evident from these figures that, irrespective of the Fe crystalline plane, in the absence of competing adsorbates (i.e. water and acid), both inhibitors adsorb almost parallel to the iron surface and the obtained distance between the inhibitors and iron surface remains virtually unchanged through the molecules. However, in the presence of water and acid, the inhibitors are adsorbed on the surface with a more tilted conformation. Such change in the adsorption configuration of inhibitors in the presence of competing molecules was theoretically and experimentally observed elsewhere [22]. As it is evident from Table 4, the rotate degrees of inhibitors in the presence of competing adsorbates are comparable for Fe (110) and Fe (−100). Due to the polycrystalline nature of mild steel and the presence of surface defects in reality inhibitors are expected to alight on the surface with a tilt angle between what is showed for different crystalline planes in Table 4.

4. Conclusion

The corrosion inhibition efficiency of two imidazole-based molecules, TCA and MTCA, on mild steel in 0.1 mol·L^{-1} HCl were investigated using electrochemical impedance spectroscopy and potentiodynamic measurements. Quantum chemical calculation was used to correlate the inhibitors' molecular structure to their corrosion inhibition efficiency. Monte Carlo simulation was performed to calculate the interaction energy between the inhibitors and metal surface in the presence and absence of competing water and acid molecules. The simulation results helped identify the most stable inhibitor conformation in each case. This information provides deeper insights into the corrosion inhibition mechanisms of the studied imidazole-based inhibitors. The following results can be summarized based on this study:

1. EIS results indicated that both TCA and MTCA show appreciable corrosion inhibition efficiencies on mild steel in HCl containing solution. The inhibition efficiencies of the studied inhibitors were improved with increasing inhibitor concentrations and reached ~90% at 150 ppm inhibitor concentration. Such inhibition efficiency is both practically and economically desirable in industrial applications.
2. Potentiodynamic polarization studies show that TCA and MTCA perform as mixed-type inhibitors by inhibiting both anodic metal dissolution and cathodic hydrogen evolution reactions. The inhibition efficiencies derived from potentiodynamic polarization measurements are in a good agreement with those obtained by EIS studies.
3. Adsorption isotherm evaluations demonstrated that both MTCA and TCA obey the Langmuir isotherm kinetics of adsorption. Based on the obtained ΔG°_{ads} values, both inhibitors adsorb though a mixed physichemisorption mechanism.
4. Quantum chemical calculation was used to determine the E_{HOMO}, E_{LUMO}, dipole moment, and Mulliken charge, confirming a strong bond between both inhibitors and metal surface.
5. MC simulation showed that both inhibitors absorb on the open structure Fe (−100) or closely packed Fe (110) surfaces with parallel orientation in the absence of water. In the presence of competing adsorbates (i.e. water and acid), the adsorption geometry of inhibitors was different, with inhibitors tilted away from the surface. The results also revealed a spontaneous adsorption process of the inhibitors on the metal surface.

Acknowledgments

The authors would like to acknowledge Mr. Ali Kosari (TU Delft, Netherlands) for helping in theoretical calculation parts and interpretation of the results and Mrs. Embrecht (FAU, Germany) for proof reading the manuscript. Mr. Iman Taji and Sohrab Pahlavan are acknowledged for valuable discussions on data analysis. SH thanks Emerging Talents Initiative (ETI) 2018/2_Tech_06, FAU, Germany grant for supporting his research.

Appendix A. Supplementary data

Supplementary data to this article can be found online at https://doi.org/10.1016/j.molliq.2019.110915.

References

[1] A. Dutta, S.K. Saha, U. Adhikari, P. Banerjee, D. Sukul, Effect of substitution on corrosion inhibition properties of 2-(substituted phenyl) benzimidazole derivatives on mild steel in 1 M HCl solution: a combined experimental and theoretical approach, Corros. Sci. 123 (2017) 256–266, https://doi.org/10.1016/j.corsci.2017.04.017.
[2] C. Verma, J. Haque, M.A. Quraishi, E.E. Ebenso, Aqueous phase environmental friendly organic corrosion inhibitors derived from one step multicomponent reactions: a review, J. Mol. Liq. 275 (2019) 18–40, https://doi.org/10.1016/j.molliq.2018.11.040.
[3] S.K. Saha, P. Banerjee, Introduction of newly synthesized Schiff base molecules as efficient corrosion inhibitors for mild steel in 1 M HCl medium: an experimental, density functional theory and molecular dynamics simulation study, Mater. Chem. Front. 2 (2018) 1674–1691, https://doi.org/10.1039/C8QM00162F.
[4] L. Wang, Evaluation of 2-mercaptobenzimidazole as corrosion inhibitor for mild steel in phosphoric acid, Corros. Sci. 43 (2001) 2281–2289, https://doi.org/10.1016/S0010-938X(01)00036-1.
[5] M.A. Quraishi, d. Jamal, Inhibition of mild steel corrosion in the presence of fatty acid triazoles, J. Appl. Electrochem. 32 (2002) 425–430, https://doi.org/10.1023/A:1016348710085.
[6] I.B. Obot, Z.M. Gasem, Theoretical evaluation of corrosion inhibition performance of some pyrazine derivatives, Corros. Sci. 83 (2014) 359–366, https://doi.org/10.1016/j.corsci.2014.03.008.
[7] J.O. Mendes, E.C. da Silva, A.B. Rocha, On the nature of inhibition performance of imidazole on iron surface, Corros. Sci. 57 (2012) 254–259, https://doi.org/10.1016/j.corsci.2011.12.011.
[8] A. Popova, M. Christov, S. Raicheva, E. Sokolova, Adsorption and inhibitive properties of benzimidazole derivatives in acid mild steel corrosion, Corros. Sci. 46 (2004) 1333–1350, https://doi.org/10.1016/j.corsci.2003.09.025.

[9] K.F. Khaled, The inhibition of benzimidazole derivatives on corrosion of iron in 1 M HCl solutions, Electrochim. Acta 48 (2003) 2493–2503, https://doi.org/10.1016/S0013-4686(03)00291-3.

[10] S. Varvara, L.M. Muresan, K. Rahmouni, H. Takenouti, Evaluation of some non-toxic thiadiazole derivatives as bronze corrosion inhibitors in aqueous solution, Corros. Sci. 50 (2008) 2596–2604, https://doi.org/10.1016/j.corsci.2008.06.046.

[11] L.M. Rodríguez-Valdez, W. Villamisar, M. Casales, J.G. González-Rodriguez, A. Martínez-Villafañe, L. Martinez, D. Glossman-Mitnik, Computational simulations of the molecular structure and corrosion properties of amidoethyl, aminoethyl and hydroxyethyl imidazolines inhibitors, Corros. Sci. 48 (2006) 4053–4064, https://doi.org/10.1016/j.corsci.2006.05.036.

[12] F. Bentiss, F. Gassama, d. Barbry, L. Gengembre, H. Vezin, M. Lagrenée, M. Traisnel, Enhanced corrosion resistance of mild steel in molar hydrochloric acid solution by 1,4-bis(2-pyridyl)-5H-pyridazino[4,5-b]indole: electrochemical, theoretical and XPS studies, Appl. Surf. Sci. 252 (2006) 2684–2691, https://doi.org/10.1016/j.apsusc.2005.03.231.

[13] A. Dutta, S.K. Saha, P. Banerjee, D. Sukul, Correlating electronic structure with corrosion inhibition potentiality of some bis-benzimidazole derivatives for mild steel in hydrochloric acid: combined experimental and theoretical studies, Corros. Sci. 98 (2015) 541–550, https://doi.org/10.1016/j.corsci.2015.05.065.

[14] C. Verma, H. Lgaz, D.K. Verma, E.E. Ebenso, I. Bahadur, M.A. Quraishi, Molecular dynamics and Monte Carlo simulations as powerful tools for study of interfacial adsorption behavior of corrosion inhibitors in aqueous phase: a review, J. Mol. Liq. 260 (2018) 99–120, https://doi.org/10.1016/j.molliq.2018.03.045.

[15] S.K. Saha, M. Murmu, N.C. Murmu, P. Banerjee, Evaluating electronic structure of quinazolinone and pyrimidinone molecules for its corrosion inhibition effectiveness on target specific mild steel in the acidic medium: a combined DFT and MD simulation study, J. Mol. Liq. 224 (2016) 629–638, https://doi.org/10.1016/j.molliq.2016.09.110.

[16] S.K. Saha, M. Murmu, N.C. Murmu, I.B. Obot, P. Banerjee, Molecular level insights for the corrosion inhibition effectiveness of three amine derivatives on the carbon steel surface in the adverse medium: a combined density functional theory and molecular dynamics simulation study, Surf. Interface Anal. 10 (2018) 65–73, https://doi.org/10.1016/j.surfin.2017.11.007.

[17] M. Murmu, S.K. Saha, N.C. Murmu, P. Banerjee, Effect of stereochemical conformation into the corrosion inhibitive behaviour of double azomethine based Schiff bases on mild steel surface in 1 Mol L−1 HCl medium: an experimental, density functional theory and molecular dynamics simulation study, Corros. Sci. 146 (2019) 134–151, https://doi.org/10.1016/j.corsci.2018.10.002.

[18] E.S.H. El Ashry, A. El Nemr, S.A. Esawy, S. Ragab, Corrosion inhibitors, Electrochim. Acta 51 (2006) 3957–3968, https://doi.org/10.1016/j.electacta.2005.11.010.

[19] I.B. Obot, N.O. Obi-Egbedi, Fluconazole as an inhibitor for aluminium corrosion in 0.1M HCl, Colloids Surf. A Physicochem. Eng. Asp. 330 (2008) 207–212, https://doi.org/10.1016/j.colsurfa.2008.07.058.

[20] N. Khalil, Quantum chemical approach of corrosion inhibition, Electrochim. Acta 48 (2003) 2635–2640, https://doi.org/10.1016/S0013-4686(03)00307-4.

[21] M. Özcan, İ. Dehri, Electrochemical and quantum chemical studies of some Sulphur-containing organic compounds as inhibitors for the acid corrosion of mild steel, Prog. Org. Coat. 51 (2004) 181–187, https://doi.org/10.1016/j.porgcoat.2004.07.017.

[22] E. Naseri, M. Hajisafari, A. Kosari, M. Talari, S. Hosseinpour, A. Davoodi, Inhibitive effect of Clopidogrel as a green corrosion inhibitor for mild steel; statistical modeling and quantum Monte Carlo simulation studies, J. Mol. Liq. 269 (2018) 193–202, https://doi.org/10.1016/j.molliq.2018.08.050.

[23] J. Zhou, S. Chen, L. Zhang, Y. Feng, H. Zhai, Studies of protection of self-assembled films by 2-mercapto-5-methyl-1,3,4-thiadiazole on iron surface in 0.1M H2SO4 solutions, J. Electroanal. Chem. 612 (2008) 257–268, https://doi.org/10.1016/j.jelechem.2007.10.011.

[24] E.E. Oguzie, C.K. Enenebeaku, C.O. Akalezi, S.C. Okoro, A.A. Ayuk, E.N. Ejike, Adsorption and corrosion-inhibiting effect of Dacryodis edulis extract on low-carbon-steel corrosion in acidic media, J. Colloid Interface Sci. 349 (2010) 283–292, https://doi.org/10.1016/j.jcis.2010.05.027.

[25] K.F. Khaled, M.A. Amin, Corrosion monitoring of mild steel in sulphuric acid solutions in presence of some thiazole derivatives – molecular dynamics, chemical and electrochemical studies, Corros. Sci. 51 (2009) 1964–1975, https://doi.org/10.1016/j.corsci.2009.05.023.

[26] L. Guo, S. Zhu, S. Zhang, Q. He, W. Li, Theoretical studies of three triazole derivatives as corrosion inhibitors for mild steel in acidic medium, Corros. Sci. 87 (2014) 366–375, https://doi.org/10.1016/j.corsci.2014.06.040.

[27] L.O. Olasunkanmi, B.P. Moloto, I.B. Obot, E.E. Ebenso, Anticorrosion studies of some hydantoin derivatives for mild steel in 0.5 M HCl solution: experimental, quantum chemical, Monte Carlo simulations and QSAR studies, J. Mol. Liq. 252 (2018) 62–74, https://doi.org/10.1016/j.molliq.2017.11.169.

[28] C. Verma, I.B. Obot, I. Bahadur, E.-S.M. Sherif, E.E. Ebenso, Choline based ionic liquids as sustainable corrosion inhibitors on mild steel surface in acidic medium: gravimetric, electrochemical, surface morphology, DFT and Monte Carlo simulation studies, Appl. Surf. Sci. 457 (2018) 134–149, https://doi.org/10.1016/j.apsusc.2018.06.035.

[29] H. Hamani, T. Douadi, M. Al-Noaimi, S. Issaadi, D. Daoud, S. Chafaa, Electrochemical and quantum chemical studies of some azomethine compounds as corrosion inhibitors for mild steel in 1M hydrochloric acid, Corros. Sci. 88 (2014) 234–245, https://doi.org/10.1016/j.corsci.2014.07.044.

[30] A.Y. Musa, A.A.H. Kadhum, A.B. Mohamad, A.A.B. Rahoma, H. Mesmari, Electrochemical and quantum chemical calculations on 4,4-dimethyloxazolidine-2-thione as inhibitor for mild steel corrosion in hydrochloric acid, J. Mol. Struct. 969 (2010) 233–237, https://doi.org/10.1016/j.molstruc.2010.02.051.

[31] R. Dennington, T. Keith, J. Millam, GaussView, version 5, Semichem Inc., Shawnee Mission. KS, 2009.

[32] A. Singh, K.R. Ansari, M.A. Quraishi, H. Lgaz, Y. Lin, Synthesis and investigation of pyran derivatives as acidizing corrosion inhibitors for N80 steel in hydrochloric acid: theoretical and experimental approaches, J. Alloys Compd. 762 (2018) 347–362, https://doi.org/10.1016/j.jallcom.2018.05.236.

[33] I.B. Obot, S. Kaya, C. Kaya, B. Tüzün, Density functional theory (DFT) modeling and Monte Carlo simulation assessment of inhibition performance of some carbohydrazide Schiff bases for steel corrosion, Physica E 80 (2016) 82–90, https://doi.org/10.1016/j.physe.2016.01.024.

[34] Y. Sasikumar, A.S. Adekunle, L.O. Olasunkanmi, I. Bahadur, R. Baskar, M.M. Kabanda, I.B. Obot, E.E. Ebenso, Experimental, quantum chemical and Monte Carlo simulation studies on the corrosion inhibition of some alkyl imidazolium ionic liquids containing tetrafluoroborate anion on mild steel in acidic medium, J. Mol. Liq. 211 (2015) 105–118, https://doi.org/10.1016/j.molliq.2015.06.052.

[35] R.L.C. Akkermans, N.A. Spenley, S.H. Robertson, Monte Carlo methods in materials studio, Mol. Simul. 39 (2013) 1153–1164, https://doi.org/10.1080/08927022.2013.843775.

[36] K.F. Khaled, Monte Carlo simulations of corrosion inhibition of mild steel in 0.5 M sulphuric acid by some green corrosion inhibitors, J. Solid State Electrochem. 13 (2009) 1743–1756, https://doi.org/10.1007/s10008-009-0845-y.

[37] A. Döner, R. Solmaz, M. Özcan, G. Kardaş, Experimental and theoretical studies of thiazoles as corrosion inhibitors for mild steel in sulphuric acid solution, Corros. Sci. 53 (2011) 2902–2913, https://doi.org/10.1016/j.corsci.2011.05.027.

[38] H. Ashassi-Sorkhabi, E. Asghari, Effect of hydrodynamic conditions on the inhibition performance of l-methionine as a “green” inhibitor, Electrochim. Acta 54 (2008) 162–167, https://doi.org/10.1016/j.electacta.2008.08.024.

[39] A. Popova, M. Christov, Evaluation of impedance measurements on mild steel corrosion in acid media in the presence of heterocyclic compounds, Corros. Sci. 48 (2006) 3208–3221, https://doi.org/10.1016/j.corsci.2005.11.001.

[40] C.M. Goulart, A. Esteves-Souza, C.A. Martinez-Huitle, C.J.F. Rodrigues, M.A.M. Maciel, A. Echevarria, Experimental and theoretical evaluation of semicarbazones and thiosemicarbazones as organic corrosion inhibitors, Corros. Sci. 67 (2013) 281–291, https://doi.org/10.1016/j.corsci.2012.10.029.

[41] A.Y. Musa, A.A.H. Kadhum, A.B. Mohamad, M.S. Takriff, Experimental and theoretical study on the inhibition performance of triazole compounds for mild steel corrosion, Corros. Sci. 52 (2010) 3331–3340, https://doi.org/10.1016/j.corsci.2010.06.002.

[42] Z. Zhang, N. Tian, W. Zhang, X. Huang, Le Ruan, L. Wu, Inhibition of carbon steel corrosion in phase-change-materials solution by methionine and proline, Corros. Sci. 111 (2016) 675–689, https://doi.org/10.1016/j.corsci.2016.06.005.

[43] S.K. Shukla, M.A. Quraishi, Cefalexin drug: a new and efficient corrosion inhibitor for mild steel in hydrochloric acid solution, Mater. Chem. Phys. 120 (2010) 142–147, https://doi.org/10.1016/j.matchemphys.2009.10.037.

[44] J. Aljourani, K. Raeissi, M.A. Golozar, Benzimidazole and its derivatives as corrosion inhibitors for mild steel in 1M HCl solution, Corros. Sci. 51 (2009) 1836–1843, https://doi.org/10.1016/j.corsci.2009.05.011.

[45] A. Kosari, M.H. Moayed, A. Davoodi, R. Parvizi, M. Momeni, H. Eshghi, H. Moradi, Electrochemical and quantum chemical assessment of two organic compounds from pyridine derivatives as corrosion inhibitors for mild steel in HCl solution under stagnant condition and hydrodynamic flow, Corros. Sci. 78 (2014) 138–150, https://doi.org/10.1016/j.corsci.2013.09.009.

[46] J. Fang, J. Li, Quantum chemistry study on the relationship between molecular structure and corrosion inhibition efficiency of amides, J. Mol. Struct. THEOCHEM 593 (2002) 179–185, https://doi.org/10.1016/S0166-1280(02)00316-0.

[47] G. Bereket, E. Hür, C. Öğretir, Quantum chemical studies on some imidazole derivatives as corrosion inhibitors for iron in acidic medium, J. Mol. Struct. THEOCHEM 578 (2002) 79–88, https://doi.org/10.1016/S0166-1280(01)00684-4.

[48] Y. Qiang, S. Zhang, L. Guo, X. Zheng, B. Xiang, S. Chen, Experimental and theoretical studies of four allyl imidazolium-based ionic liquids as green inhibitors for copper corrosion in sulfuric acid, Corros. Sci. 119 (2017) 68–78, https://doi.org/10.1016/j.corsci.2017.02.021.

[49] T. Arslan, F. Kandemirli, E.E. Ebenso, I. Love, H. Alemu, Quantum chemical studies on the corrosion inhibition of some sulphonamides on mild steel in acidic medium, Corros. Sci. 51 (2009) 35–47, https://doi.org/10.1016/j.corsci.2008.10.016.

[50] A.Y. Musa, A.A.H. Kadhum, A.B. Mohamad, M.S. Takriff, Molecular dynamics and quantum chemical calculation studies on 4,4-dimethyl-3-thiosemicarbazide as corrosion inhibitor in 2.5M H2SO4, Mater. Chem. Phys. 129 (2011) 660–665, https://doi.org/10.1016/j.matchemphys.2011.05.010.

[51] F.E. Hajjaji, M.E. Belghiti, B. Hammouti, S. Jodeh, O. Hamed, H. Lgaz, R. Salghi, Adsorption and corrosion inhibition effect of 2-Mercaptobenzimidazole (surfactant) on a carbon steel surface in an acidic medium: experimental and Monte Carlo simulations, Port. Electrochim. Acta 36 (2018) 197–212, https://doi.org/10.4152/pea.201803197.